

Seismic Response of Irregular Triangular Alluvial Valleys under Shear Waves Using Spectral Elements

Saeed Hosseinpour ^{a*}, Jafar Najafizadeh ^a

^a Department of Civil Engineering, Bojnourd Branch, Islamic Azad University, Bojnourd, Iran.

Received 17 June 2018; Accepted 03 October 2018

Abstract

The present study investigates seismic response problems of triangular uniform irregular alluvial valleys under shear waves using a finite element spectral method. Alluvial valleys; affect the shape and properties of alluvial materials on the response and seismic behavior of the valley surface due to the geometry conditions. Therefore this study aims to illustrate the plots and magnitude of amplification values for irregular alluvial valleys in a two-dimensional triangular manner, with the characteristics of homogeneous alluvial materials and different geometric characteristics. The analysis in the time domain was performed based on the finite element method of the spectral element (SFEM) using NASEM software, developed by Najafizadeh. The valleys are analyzed with the slope angles of 15, 30, 45 and 60 degrees on one side and in opposite directions with a slope of 45 degrees and with a maximum depth of 50 meters for the alluvial valley. The horizontal amplification curves in the alluvial valley's points from the analysis reach a maximum value at a given frequency, which can be an ideology for determining the frequency of irregular triangular alluvial valleys under different slope valley angles. The results of natural valley frequencies indicate that with decreasing slope of the valley, the natural frequency of the valley decreases, as well as amplification plots are related to the slope of the valley.

Keywords: Irregular Triangular Alluvial Valleys; Horizontal Amplification; Topographic Effects; Spectral Finite Elements; Seismic Response; Shear Invasive Waves.

1. Introduction

In many studies, the effects of site topography on response and seismic behavior have been studied. Most of these studies were based on the regularity of the site and the proposed methods and models were based on the regularity of topographic complications such as hills and valleys. In the case of an irregular topography of a valley or hill, its effects on seismic response should be investigated and the effects of irregular topography on the response and seismic behavior of the site should be examined. The complexity of the seismic response of topographic complications and especially the irregularities of topographic complications shows the necessity of studying seismic responses of these types of complications, using appropriate numerical methods. Therefore, the use of a suitable numerical method is important, which in addition to solving the equations governing the propagation of waves, considers the effects of topography, soil layers and so on. In addition, a method that can model all the details required for the propagation of waves in the effects of the earth's topography with a high precision and reducing computational operations, which reduces the time and cost of the analyzes and has a good rate of speed in this regard is also important. The application and use of numerical methods in topographic complications have increased over the past two decades, and most of these methods have become operational. Some of these methods did not have the ability to perform complex modeling and did not have a proper performance by increasing the researchers' awareness of the nature of the waves and the structure of the topographic

* Corresponding author: s.hp1992@yahoo.com

 <http://dx.doi.org/10.28991/cej-03091189>

➤ This is an open access article under the CC-BY license (<https://creativecommons.org/licenses/by/4.0/>).

© Authors retain all copyrights.

complications. In addition, because numerical models made with large dimensions are important for wave propagation problems in the site, and also researchers have always been looking for new, high-speed numerical methods in computing with the advancement of powerful computer technology. Among the advanced numerical methods that researchers have used in the seismic behavior of site topographic complications, the finite element method, or the combination of these two methods can be referred.

Combined techniques are a combination of various techniques that are used to enhance numerical analysis capabilities and to overcome the limitations of each numerical method. Among the researchers who used this method, we can refer to Ohtsuki and Harumi [1] and Ohtsuki et al. [2], which combines the numerical finite element and finite difference methods to study and study the effects of topography and ground-level inhomogeneity against SV and Reighly shear invasive waves. Chuhan and Chongbin [3] combined the finite and unlimited elements of the surface topography of valleys against SH shear invasive waves. Sohrabi and Kamalian [4] proposed the combination of finite element and boundary element methods and the development of a hybrid program to solve the seismic response problems of topographic complications of hills and valleys.

In 2018, Ling Ning and colleagues investigated the propagation of Rayleigh waves in two-dimensional valleys using the Finite-difference valves and showed that the propagation of Riley waves at high frequencies plays an important and important role in earthquake response. And its effect on the topography of the valleys is more than the hills [5]. In 2018, Zezhong Zhang and colleagues looked at the magnitude of the gradient pattern under the invasive wave of the SV and showed that the largest magnification pattern was obtained at a 32.3-degree gradient and would not necessarily occur at the tilt peaks [6]. Rinousau et al. (1997) studied the direct boundary integral method for the issue of two-dimensional wave propagation for the Riley, SV and P wave in the Mexico City valley. Atanasopoulos et al. investigated the topographic effects on the earth's earthquake response in the Ajuvan region of Greece (based on the 1995 earthquake using finite element method) [7]. Todo et al. (2001), the boundary element method for various frequencies and harmonic loading, they studied the propagation of three-dimensional waves produced by expanding a point in an infinite half-space [8].

Ali Kavand et al. (2016) investigated the seismic response of alluvial deposits due to the vertical component of earthquakes near the fault zone. In this article, the local effects of the site on the characteristics of the vertical component of accelerated earthquakes in the field are investigated. The results show that the ratio of vertical to horizontal velocity (v/h) is influenced by factors such as the basic period of the vibrational structure of the site in the mode of compression wave propagation, the Poisson ratio of the soil, and also the characteristics of the stimulus input [9].

Najafzadeh et al., in 2014 and 2015 solved wave propagation problems in topographic effects of rectangular valleys, using numerical finite element method and writing NASEM program, and studied the rectangular valley amplification pattern. They also examined the amplification pattern of the rectangular shape of the alluvial valley under the SV vertical shear waves in both linear and nonlinear states, and showed a comprehensive relationship for the natural frequency of the rectangular alluvial valley [10, 11]. In this study, the seismic response behavior of irregular triangular alluvial valleys under SV shear invasive waves using the spatial finite element method (SFEM) method have been investigated to determine the various influential factors and parameters on the response of irregular triangular alluvial valleys against SV shear invasive waves with different slope angles of the valley. Three effects are investigated in this study including the slope angle of the valley on the frequency of most triangular irregular alluvial valleys under shear invasive waves, valley irregularities on the valley elevation pattern and shear wave velocity on irregular triangular valleys. To this end, the irregular shape triangular valleys have been modeled under shear invariant waves at different angles of the slope of the valley. Then, the comprehensive and extensive numerical analyzes have been performed on the linear seismic behavior and response of these two-dimensional triangular alluvial valleys to demonstrate the effect of the above mentioned factors on the seismic response of irregular triangular alluvial valleys. The results from frequency domain research can provide a clear understanding of the variation in seismic behavior and response of irregularly shaped triangular alluvial valleys under the oblique shear wave with different angles of valley slope.

2. Research Methodology

The use of solving governing equations for wave propagation in order to model the seismic response of topographic complications has always been considered by seismologists. The purpose of this section was to find a method that is able to model all the details required for the propagation of waves in the seismic response of topographic complications, which in addition to solving this with a very high accuracy and reducing the volume of computational operations, reduces the time and has a good speed. Therefore, the method that now, in addition to solving the seismic response of topographic complications, has the proper accuracy and efficiency is the numerical method of the spectral finite element.

The purpose of the application of the spectral distribution method is to solve the Equation 1. To achieve this goal, after calculating the mass matrix and also the vector of the forces equal to the nodal element of each element, based on the degrees of release of each node and the method of placing elements in the vicinity of each other, the mass and hardness matrices and the vector of the nodal forces are aggregated so that the Relation 1 for the entire environment;

$$\int_{\Omega} \rho \cdot w \partial_t^2 s d^3x = - \int_{\Omega} \nabla w : T d^3x + M : \nabla w x_s S(t) \quad (1)$$

Finally, we arrive at the system of differential equations:

$$[M^e] \ddot{\vec{u}} + [K^e] \vec{u} + \vec{F}_t^e + \vec{F}_{ext}^e = 0 \quad (2)$$

$[M^e]$, $[K^e]$, are mass gravity matrices of each element, and \vec{F}_t^e , \vec{F}_{ext}^e , the external surface load and the load of the load on the element.

And in summing:

$$[M] = \sum_{e=1}^{n_e} [M^e] \quad , \quad [K] = \sum_{e=1}^{n_e} [K^e] \quad (3)$$

$$\vec{F}_t = \sum_{e=1}^{n_e} \vec{F}_t^e \quad , \quad \vec{F}_{ext} = \sum_{e=1}^{n_e} \vec{F}_{ext}^e$$

Thus, the system of equations governing the entire structure is as follows:

$$[M] \ddot{\vec{u}} + [K] \vec{u} + \vec{F}_t + \vec{F}_{ext} = 0 \quad (4)$$

Considering the damping of the materials, the matrix form of the above relation is written as follows:

$$[M] \ddot{\vec{u}} + [C] \dot{\vec{u}} + [K] \vec{u} = \vec{R} \quad (5)$$

$$\vec{R} = -\vec{F}_t - \vec{F}_{ext}$$

In this study, we have solved the relation with Numeric numerical method and the displacement, velocity and acceleration of all nodes at each moment of time are obtained. From these responses, strain, tension and other required answers can be quantified. In Newmark's numerical method, the damping of materials is calculated as Riley.

Steps to Solve the Newmark Method:

1. Initialize

A. Initialize change U_0 and speed \dot{U}_0 .

B. Calculate acceleration \ddot{U}_0 in time $t = 0$:

$$M \ddot{U}_0 = R^u - C \dot{U}_0 - K U_0 \quad (6)$$

C. Selecting the time step Δt , parameters α , δ and calculating the integral constants:

$$\begin{aligned} \delta \geq 0.50 \quad \alpha &\geq 0.25(0.50 + \delta)^2 \\ a_0 &= \frac{1}{\alpha \Delta t^2} \quad a_1 = \frac{\delta}{\alpha \Delta t} \quad a_2 = \frac{1}{\alpha \Delta t} \quad a_3 = \frac{1}{2\alpha} - 1 \\ a_4 &= \frac{\delta}{\alpha} - 1 \quad a_5 = \frac{\Delta t}{2} \left(\frac{\delta}{\alpha} - 2 \right) \quad a_6 = \Delta t(1 - \delta) \quad a_7 = \delta \Delta t \end{aligned} \quad (7)$$

D. Formation of Effective Hard Matrix:

$$\hat{K} = K + a_0 M + a_1 C \quad (8)$$

2. Calculations of each time step

A. Calculating Effective Times in Time $t + \Delta t$:

$$\hat{R}^u_{t+\Delta t} = R^u_{t+\Delta t} + M(a_0 U_t + a_2 \dot{U}_t + a_3 \ddot{U}_t) + C(a_1 U_t + a_4 \dot{U}_t + a_5 \ddot{U}_t) \quad (9)$$

B. Solve the following device to find the time shift $t+\Delta t$:

$$\hat{K}U_{t+\Delta t} = \hat{R}_{t+\Delta t} \tag{10}$$

C. Calculate speed and acceleration in time $t+\Delta t$:

$$\begin{aligned} \ddot{U}_{t+\Delta t} &= a_0(U_{t+\Delta t} - U_t) - a_2\dot{U}_t - a_3\ddot{U}_t \\ \dot{U}_{t+\Delta t} &= \dot{U}_t + a_6\ddot{U}_t + a_7\ddot{\ddot{U}}_{t+\Delta t} \end{aligned} \tag{11}$$

Figure 1 shows the different types of topography, surface, and sub-surface roughness including hills, valleys, slopes, sedimentary layers, faults, and alluvial valleys. The purpose of the present study was to investigate the behavior of seismic response behavior of irregular alluvial valleys of triangular shapes with different angles of slope in the valley, with a shear velocity of 300 and 400 m/s on rigid bedrock using the NASEM program based on the spectral finite element method (SFEM) [10].

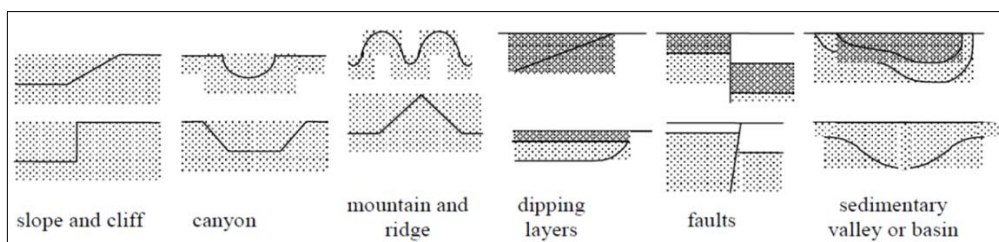


Figure 1. Different forms of surface and subsurface topography

2.1. Geometric Parameters of Alluvial Valley

In order to obtain comprehensive results, a wide range of irregular triangular alluvial valleys with slopes of 15, 30, 45, and 60 degrees on the one side of the valley and 45 degrees on the other side of the valley or with a ratio of 1.72, 0.57, and 0.27 were studied. The shape ratio here is the half-width of the valley to the thickness of the substrate. ($SR = ax/H$). The maximum thickness of the alluvial layer is 50 meters. Figure 2 shows the geometry of the valley.

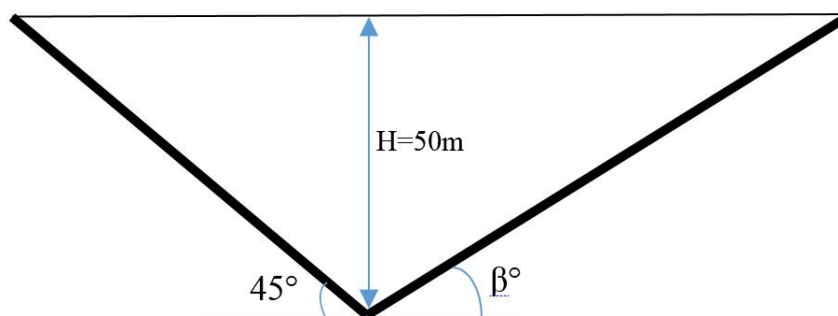


Figure 2. Schematic representation of valley geometry ($\beta = 15, 30, 45, 60^\circ$)

2.2. Mechanical Parameters of Alluvial Materials

In all models, the rigid bedrock and materials were considered as elastic and dry. The mechanical behavior of the soil was considered with the poisson ratio 0.33, the damping ratio of 0.05, and the mass density of 2 tons per cubic meter. The valleys were analyzed once at a shear wave velocity of 300 m/s and again at 400 m/s.

2.3. Invasive Wave Features

The main focus in this research is towards the behavior of the seismic response of the site (alluvial valley) due to the topographic effects under the invasive shear wave, so the simple invasive wave SV of the Ricker type is selected. Figure 3 shows the time history of the Ricker wavelet. The relationship Ricker wavelet is as follows:

$$f(t) = A_{\max} \left[1 - 2(\pi f_p (t - t_0))^2 \right] e^{-(\pi f_p (t - t_0))^2} \tag{12}$$

In which, f_p and t_0 are the predominant frequency and the time parameter in the maximum amplitude. A_{max} shows the maximum displacement in a time step. This wave of displacements is perpendicular to the direction of its propagation, due to the planar shape.

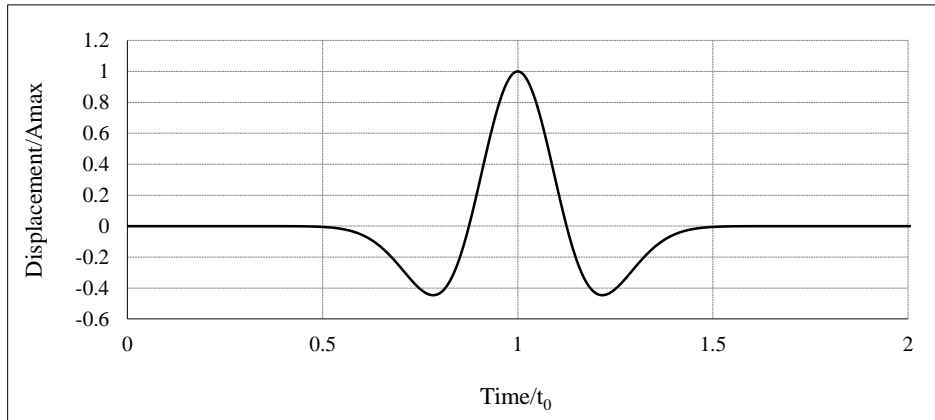
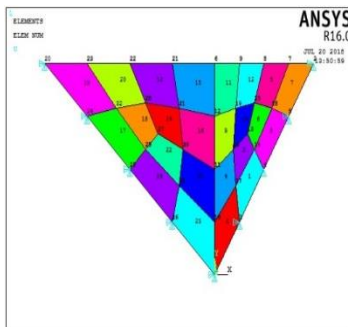


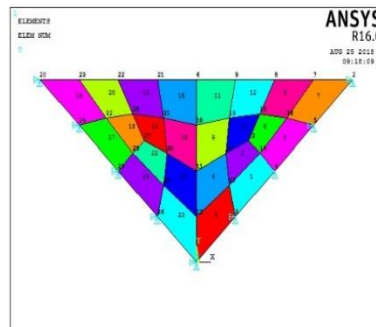
Figure 3. Ricker wavelet time history

3. Investigating the Seismic Response Results of Triangular Irregular Alluvial Valleys under Shear Invasive Waves

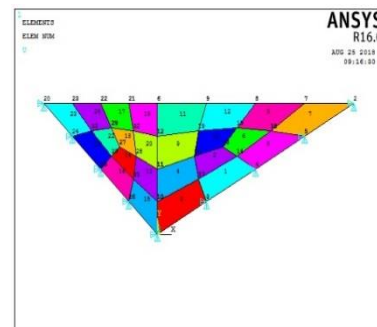
In order to investigate the seismic response of irregular alluvial valleys, a wide range of irregular triangular alluvial valleys have been investigated with linear elastic materials on a rugged rocky substrate. Initially, the models were constructed with the ANSYS software and then, analyzed with the NASEM program. Pattern and geometry of irregular triangular valleys were shown in Figure 4. The time step of the dynamic analysis was 0.055 seconds. Using the Fourier transform, the time domain was converted to the frequency domain, and the motion conversion function or seismic response is obtained by dividing the acceleration response of the ground into the acceleration input in the frequency domain. To investigate seismic response and plotting magnifications, a series of 7 points with positions $(-0.75, -0.5, -0.25, 0, 0.25, 0.5, 0.75) * X$ were selected at the valley level, where X is the distance of origin of the coordinates to the end of the valley on both sides of the valley. For example, in Figure 4-a, points 23, 22, 21, 6, 9, 8, and 7 are taken, which are numbered one to seven, respectively.



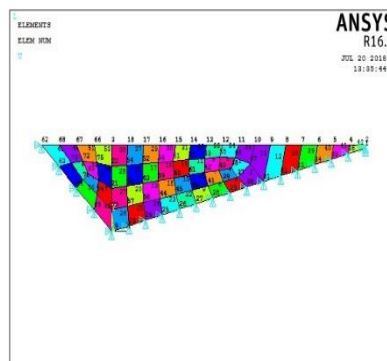
a) Meshing for $\beta = 60^\circ$



b) Meshing for $\beta = 45^\circ$



c) Meshing for $\beta = 30^\circ$



d) Meshing for $\beta = 15^\circ$

Figure 4. Meshing model

Figure 5 to 8 show the magnification pattern for irregular triangular valley areas for slope angles of 15, 30, 45, and 60 degrees. In this case, the cutting shear velocity is 300 m/s. As can be seen from the figures, the natural frequency of the irregular triangular valley decreases and moves toward the natural frequency of the soil layer on a one-dimensional stone bed by decreasing the slope of the valley. Another possible result is that the triangular has a natural frequency in each arbitrary irregular valley, which means that the natural frequency of the valley is the same on both sides of the origin of the coordinates or both sides of the vertical axis passing through the deep valley. The same results are also observed for the environment at speeds of 400 m/s (Figures 10 to 13). To better understand the irregular effects of the triangular valley on the magnitude of the valley surface.

Figures 9 and 14 are presented for both the shear velocity of 300 and 400 m/s for points 1 to 7, which were selected from the valley surface. As can be seen, with gradient angle changes (with a variation of valley irregularity) a magnification pattern of every single point in the valley is altered, so the irregular valley magnification pattern is highly dependent on the variation or irregular degree of the alluvial valley. Figures 15 to 20 are the maximum magnification comparison graphs of the various points of the alluvial valley for two environments with a shear velocity of 300 and 400 m/s. As mentioned, the magnitude of the magnification increases with decreasing slope of the irregular valley, and the slope of the valley reaches its maximum value for a 15-degree angle, which reaches a maximum of 1/3 times the maximum value in a one-dimensional model for an environment with a shear velocity of 300 m/s (Figure 16).

It should be noted that in dimensionless magnification values, magnification values obtained from the irregular valley are divided into maximum magnification values in the one-dimensional model and at the lowest angle of 60 degrees. The same thing can be seen in a shear wave velocity of 400 m/s. Here, the magnification value is 0.61 times the maximum value in the one-dimensional model. Another consequence of this problem is that the magnitude of the maximum magnification decreases with increasing shear wave velocity in the medium. In this case, it is also clear that the largest magnitudes are achieved in the right half of the valley, which has a higher weight of alluvium (from zero to one of the graphs). Figure 19 and 20 show a variation in the alluvial valley in relation to the irregular triangle slope angle for two environments with a shear velocity of 300 and 400 m/s. Table 1 shows the valley's natural frequency values for each slope of the valley. As seen from the diagrams and the table, with increasing the shear wave velocity in the environment, natural frequency increases.

Table 1. Natural frequencies for each valley slope

β^0	V_s	
	400m/s	300m/s
	f (Hz)	f (Hz)
0	2	1.5
15	3.52	2.64
30	4.4	3.32
45	5.28	3.96
60	6.25	4.69

Figure 19 shows the variation of the dimensionless natural frequency of the valley after the irregular triangular valley slope angle for two shear wave environments of 300 and 400 m/s. To obtain the natural frequency of the valley, the natural frequency of each valley was divided into the natural frequency of the one-dimensional alluvial layer. As the figure shows, the dimensionless frequency diagram for both environments with a shear velocity of 300 and 400 m/s is perfectly consistent. Therefore, it can be stated that the following equation for the natural frequency of a triangular irregular valley when a side of the valley has a slope of 45 degrees is as following:

$$f = (-2E - 7 \times \beta^4 + 3E - 5 \times \beta^3 - 0.0017 \times \beta^2 + 0.0703 \times \beta + 1) \times V_s / (4H) \quad (13)$$

Where β is the slope of the valley, V_s is the shear velocity, H is the maximum thickness of the alluvial layer of the irregular valley triangular.

Figures 5 to 8 illustrate the elevation pattern of different points of the irregular triangular valley, $V_s = 300$ m/s, at various angles of 15, 30, 45 and 60 degrees.

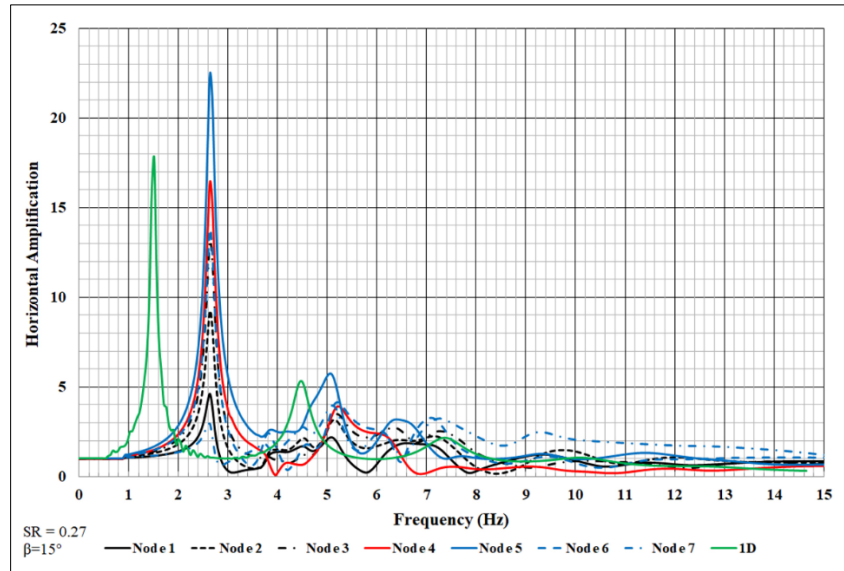


Figure 5. Amplification pattern of different points in the irregular triangular valley, $\beta=15^\circ$, $V_s=300$ m/s

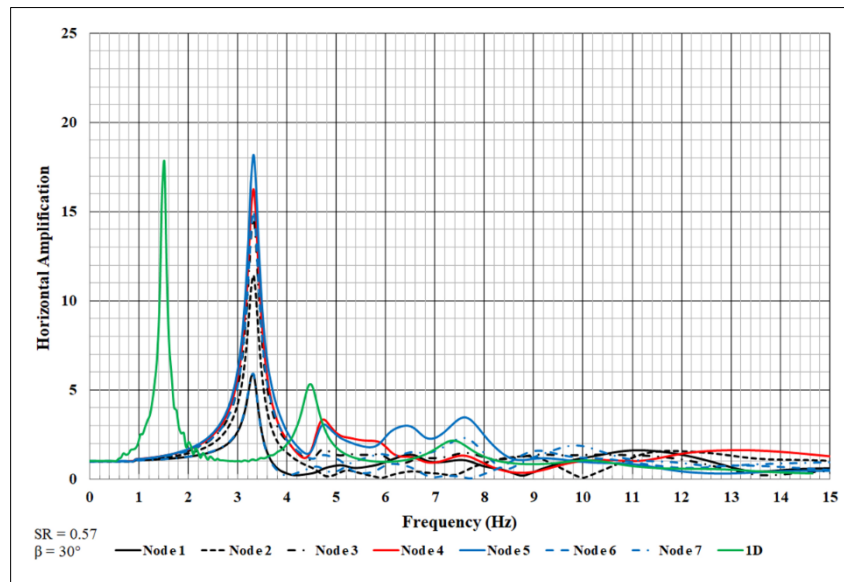


Figure 6. Amplification pattern of different points in the irregular triangular valley, $\beta=30^\circ$, $V_s=300$ m/s

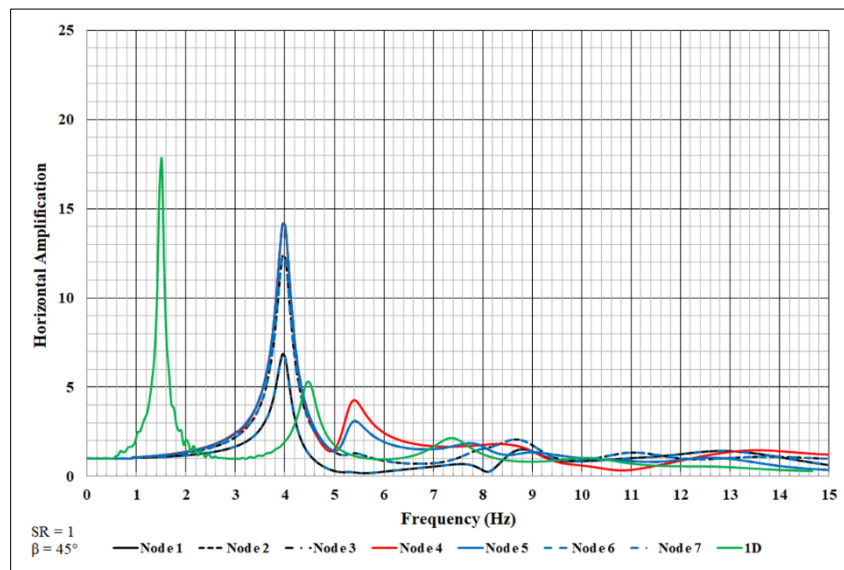


Figure 7. Amplification pattern of different points in the irregular triangular valley, $\beta=45^\circ$, $V_s=300$ m/s

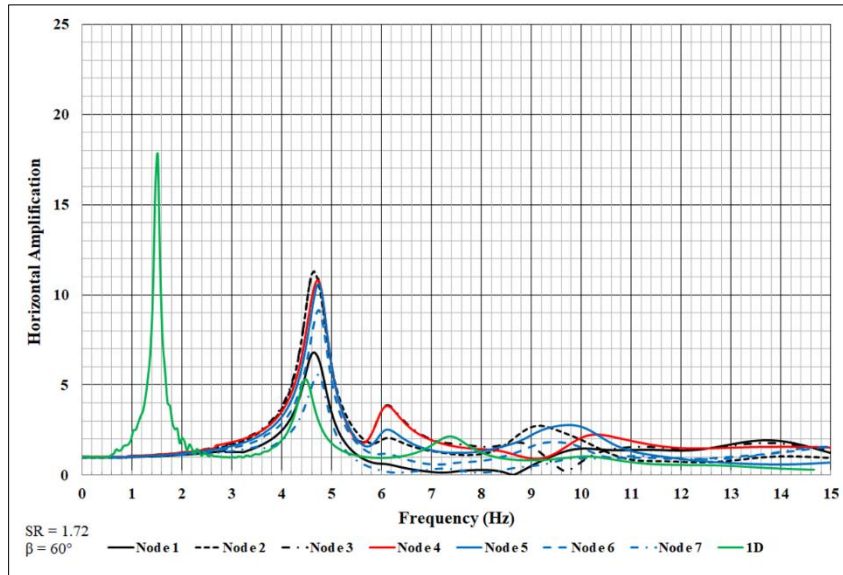
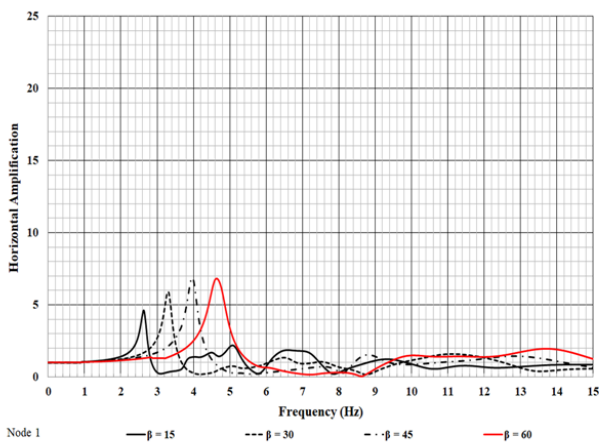
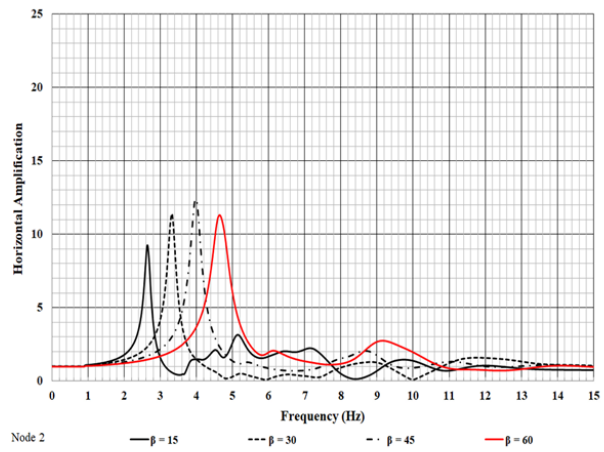


Figure 8. Amplification pattern of different points in the irregular triangular valley, $\beta=60^\circ$, $V_s=300$ m/s

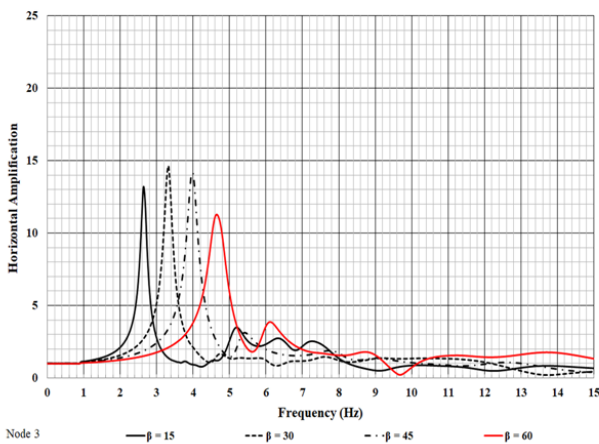
Figure 9 compares the magnification pattern of the first to seventh irregular triangular valleys at $V_s = 300$ m/s.



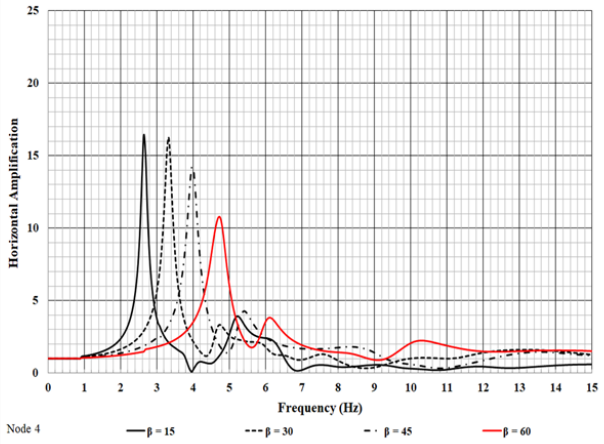
Comparison of the amplification pattern of the point number one of the irregular triangular valleys, $V_s=300$ m/s



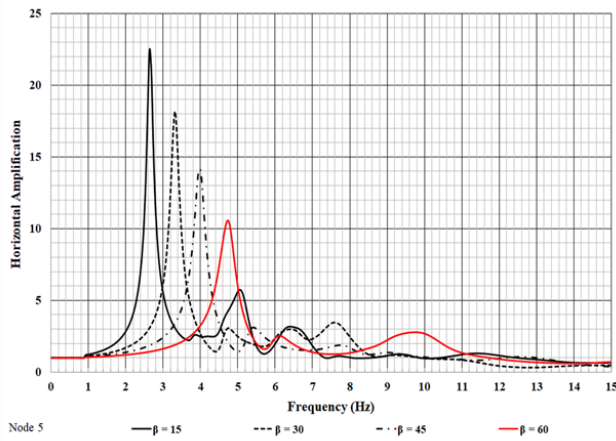
Comparison of the amplification pattern of the point number two of the irregular triangular valleys, $V_s=300$ m/s



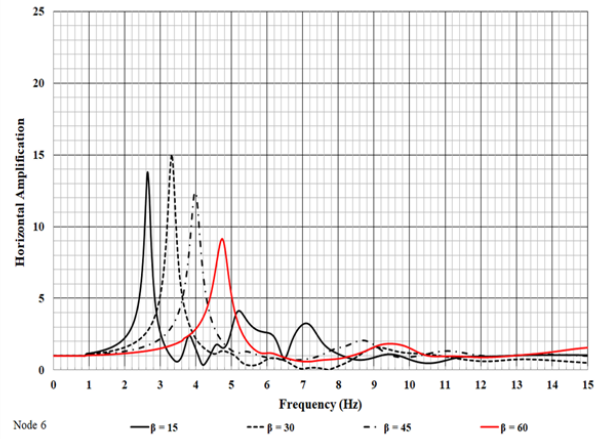
Comparison of the amplification pattern of the point number three of the irregular triangular valleys, $V_s=300$ m/s



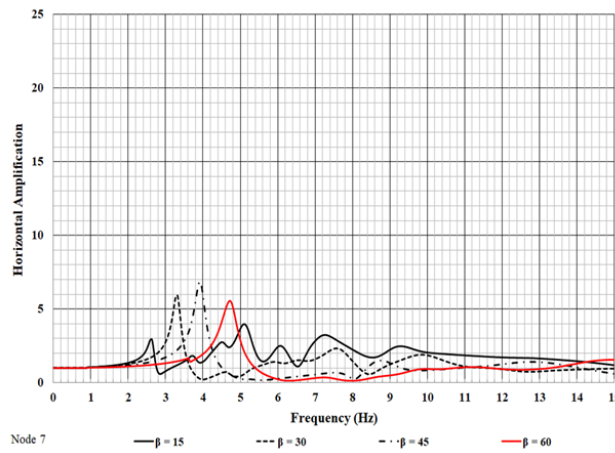
Comparison of the amplification pattern of the point number four of the irregular triangular valleys, $V_s=300$ m/s



Comparison of the amplification pattern of the point number five of the irregular triangular valleys, $V_s=300$ m/s



Comparison of the amplification pattern of the point number six of the irregular triangular valleys, $V_s=300$ m/s



Comparison of the amplification pattern of the point number seven of the irregular triangular valleys, $V_s=300$ m/s

Figure 9. Comparison of the amplification pattern of the first to seventh irregular triangular valleys $V_s = 300$ m/s

In Figures 10 to 13, the elevation pattern of different points in the irregular triangular valley is shown at $V_s = 400$ m/s at 15, 30, 45 and 60 degrees.

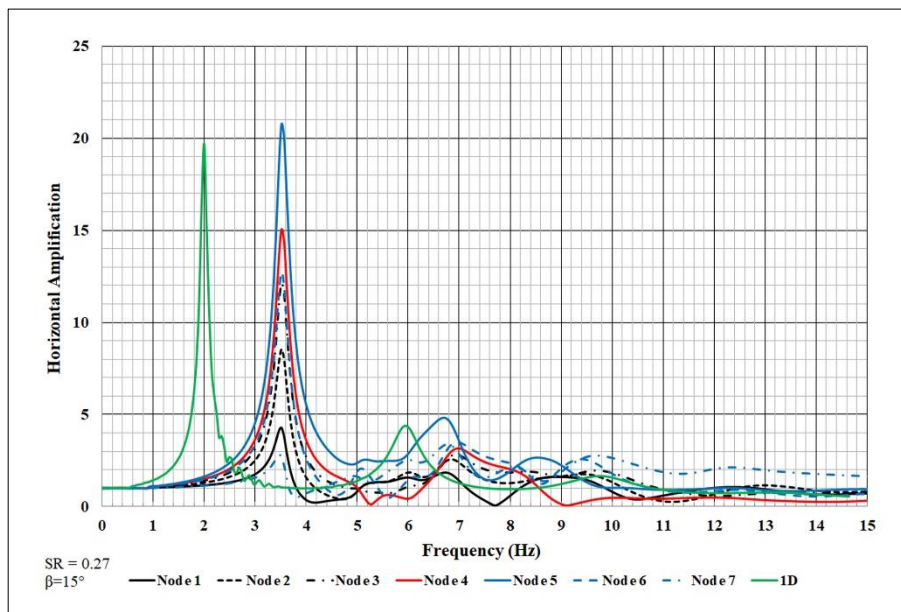


Figure 10. Amplification pattern of different points in the irregular triangular valley, $\beta=15^\circ$, $V_s=400$ m/s

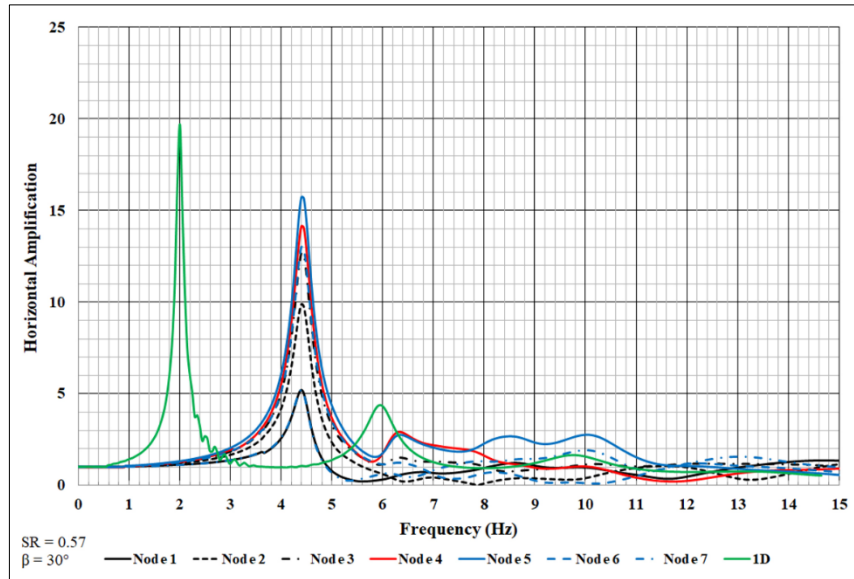


Figure 11. Amplification pattern of different points in the irregular triangular valley, $\beta=30^\circ$, $V_s=400$ m/s

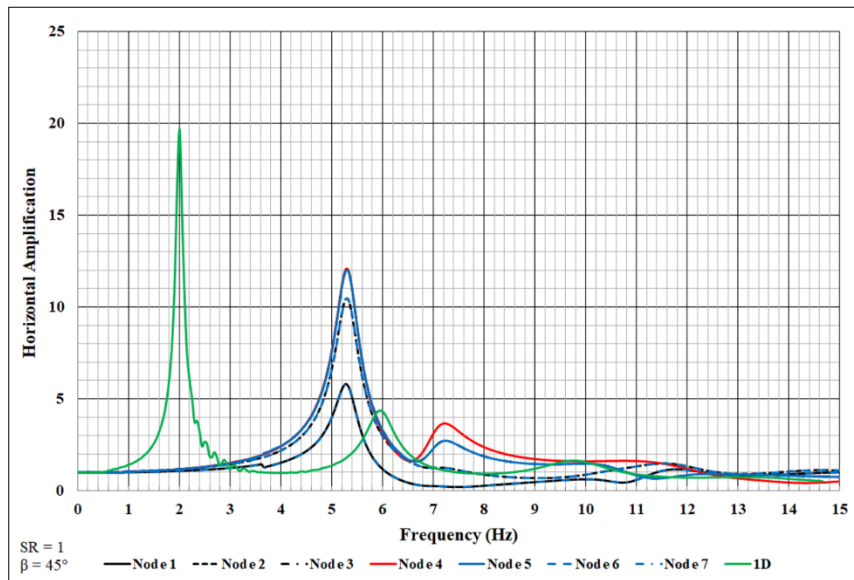


Figure 12. Amplification pattern of different points in the irregular triangular valley, $\beta=45^\circ$, $V_s=400$ m/s

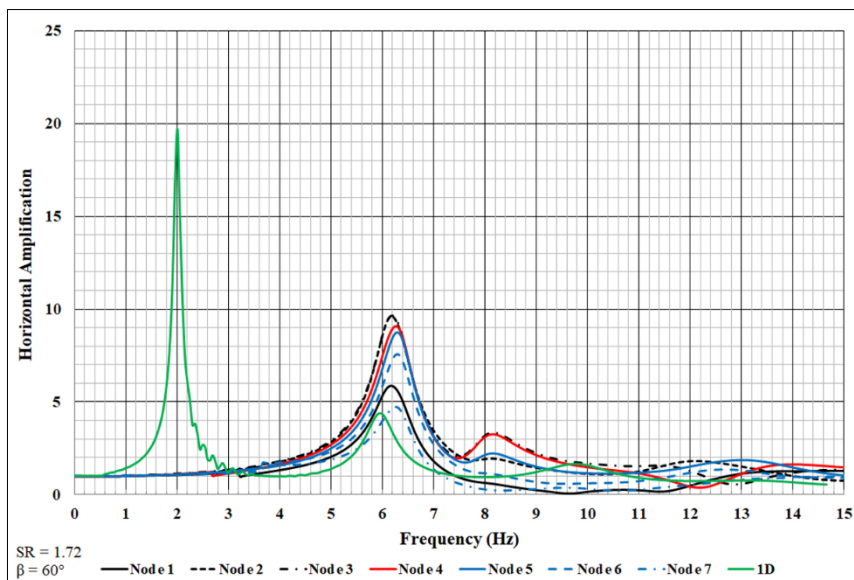
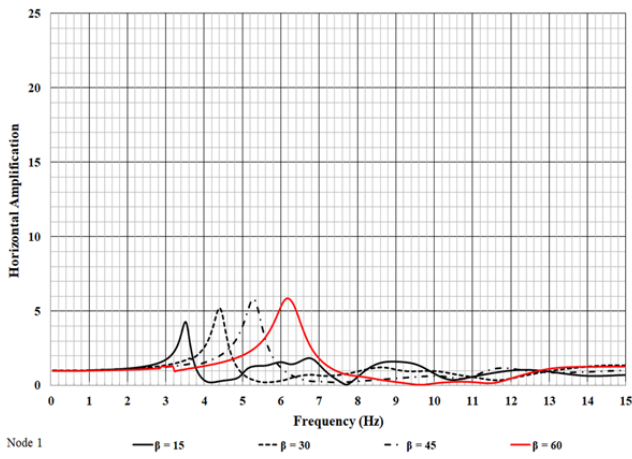
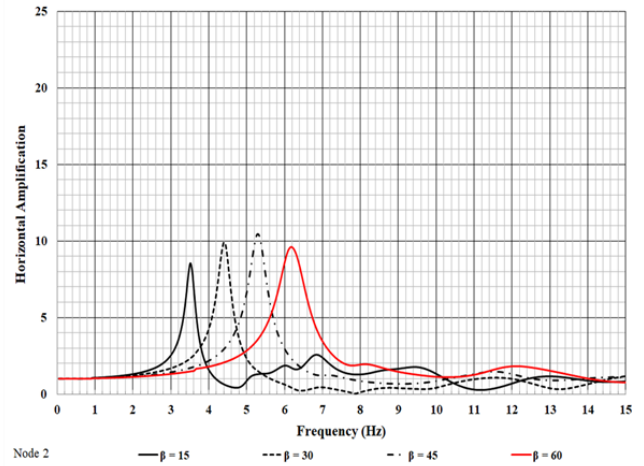


Figure 13. Amplification pattern of different points in the irregular triangular valley, $\beta=60^\circ$, $V_s=400$ m/s

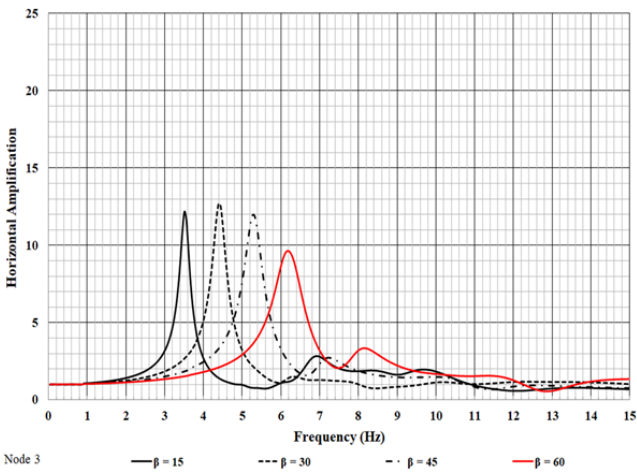
Figure 14 compares the magnification pattern of the first to seventh irregular triangular valleys at $V_s = 400$ m/s.



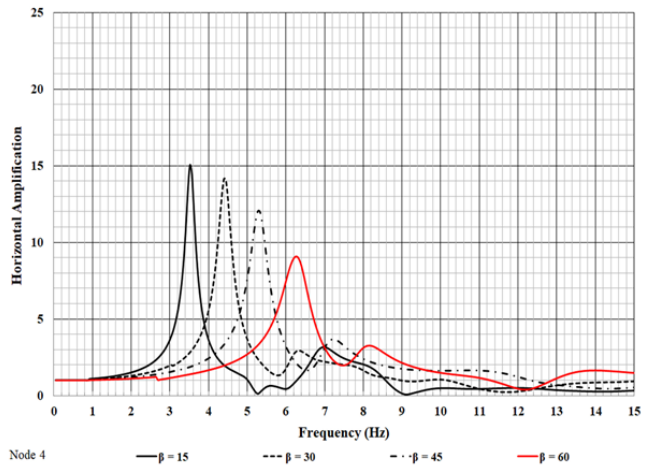
Comparison of the amplification pattern of the point number one of the irregular triangular valleys, $V_s=400$ m/s



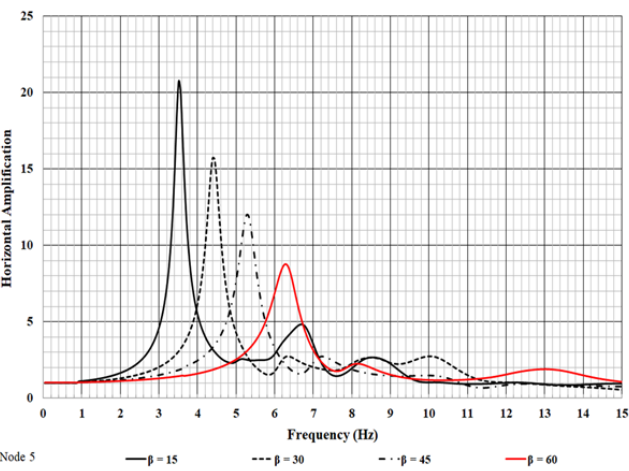
Comparison of the amplification pattern of the point number two of the irregular triangular valleys, $V_s=400$ m/s



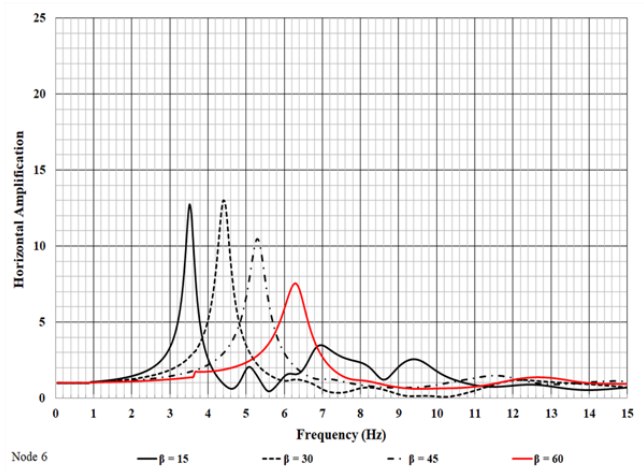
Comparison of the amplification pattern of the point number three of the irregular triangular valleys, $V_s=400$ m/s



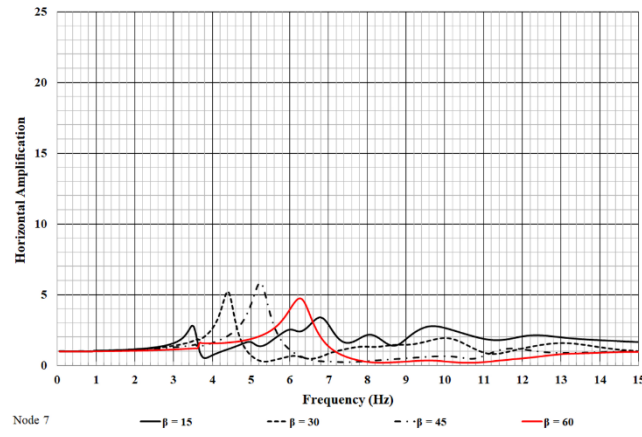
Comparison of the amplification pattern of the point number four of the irregular triangular valleys, $V_s=400$ m/s



Comparison of the amplification pattern of the point number five of the irregular triangular valleys, $V_s=400$ m/s



Comparison of the amplification pattern of the point number six of the irregular triangular valleys, $V_s=400$ m/s



Comparison of the amplification pattern of the point number seven of the irregular triangular valleys, $V_s=400$ m/s

Figure 14. Comparison of the amplification pattern of the first to seventh irregular triangular valleys $V_s = 300$ m/s

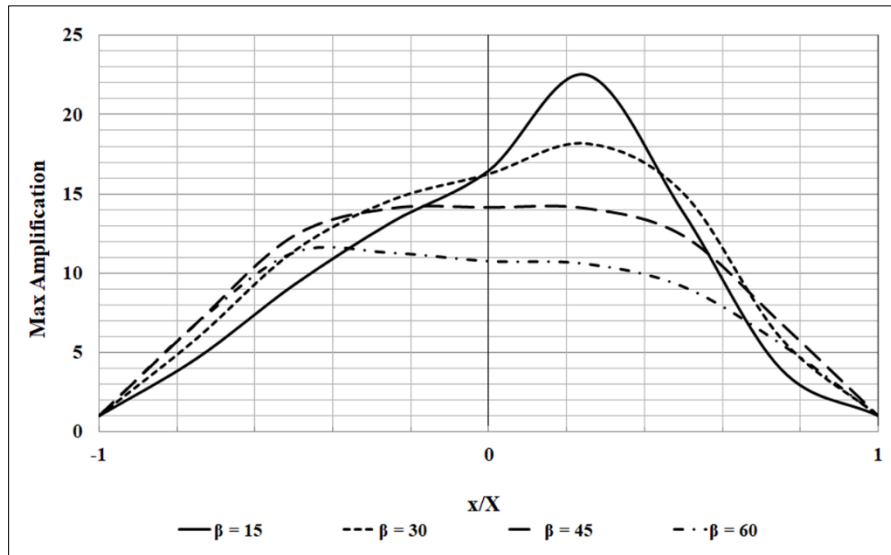


Figure 15. Comparison of maximum amplification values of irregular triangular valley points, $V_s = 300$ m/s

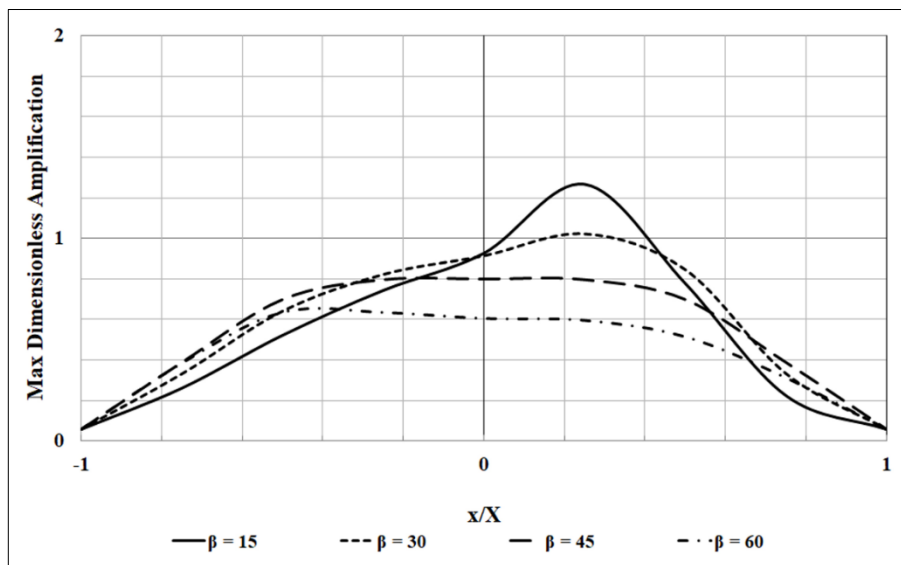


Figure 16. Comparison of the maximum dimensionless amplification values of irregular triangular valley points, $V_s = 300$ m/s

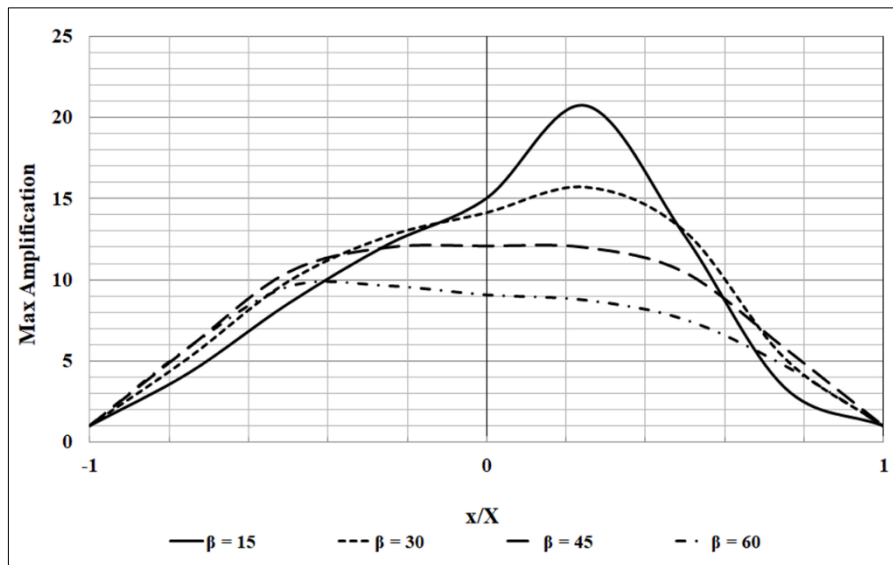


Figure 17. Comparison of maximum amplification values of irregular valley triangular points, $V_s = 400$ m/s

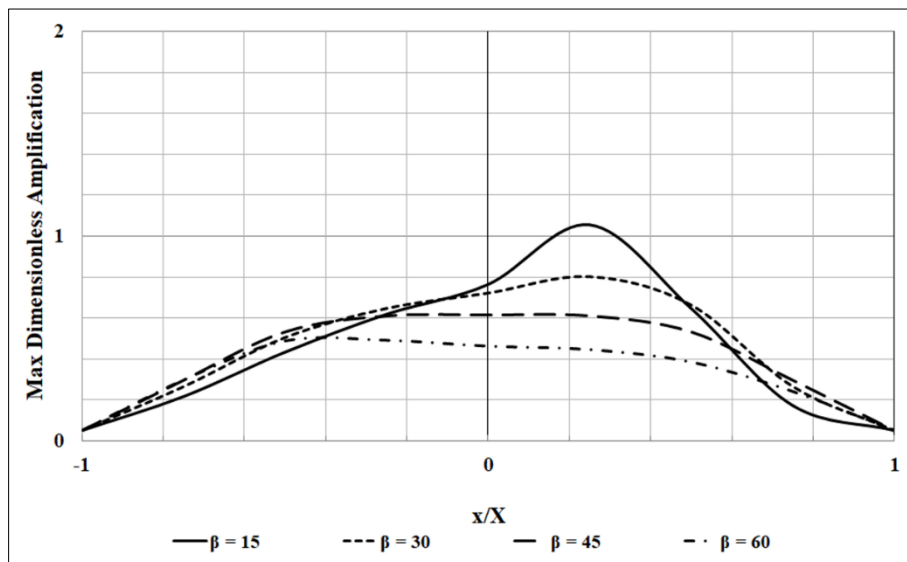


Figure 18. Comparison of maximum dimensionless amplification values of irregular valley triangular points, $V_s = 400$ m/s

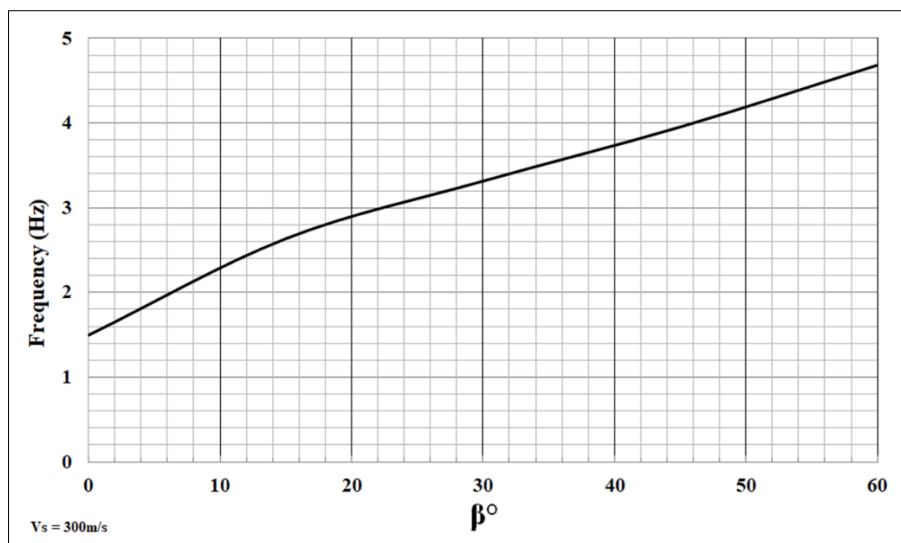


Figure 19. Frequency variations vs slope angle of triangular irregular valley, $V_s = 300$ m/s

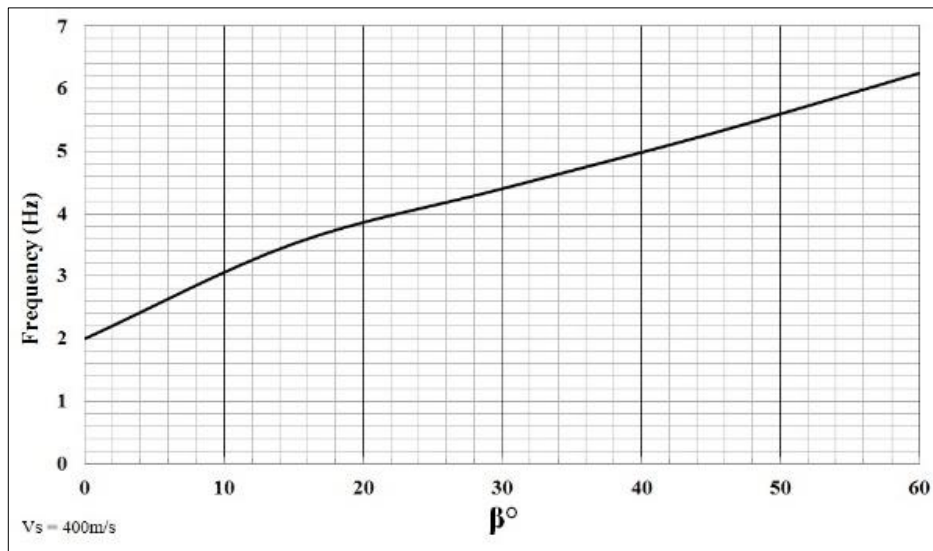


Figure 20. Frequency variations vs slope angle of triangular irregular valley, $V_s = 400 \text{ m/s}$

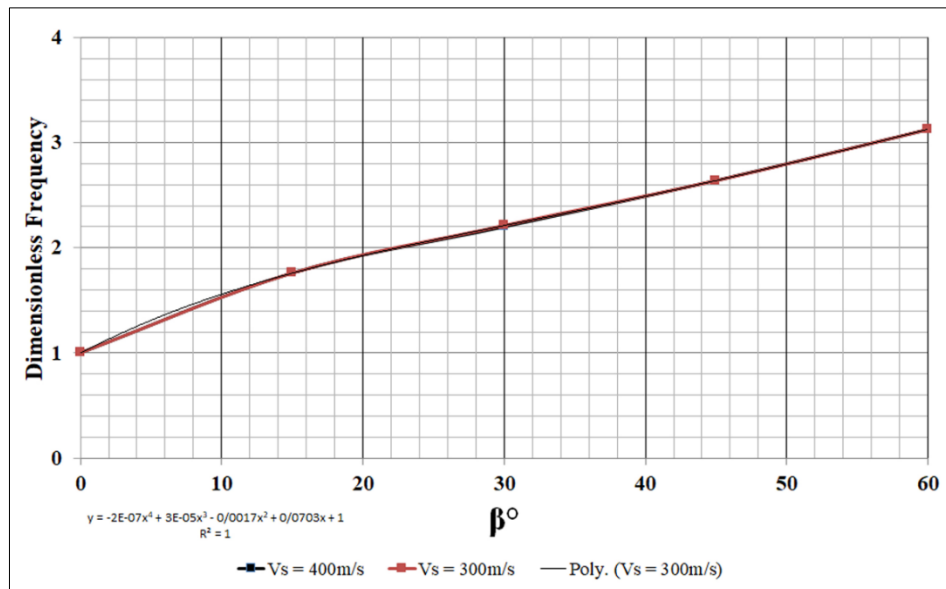


Figure 21. Dimensionless frequency variations vs slope angle of triangular irregular valley

4. Conclusion

The seismic response of irregular triangular alluvial valleys is strongly affected by geometry, the mechanical properties of the alluvial valley, and the type and angle of the invasive wave in that valley. Seismic waves into the valley alluvial are greatly influenced by collisions with topography geometry and alluvial materials. To accurately analyze the seismic response of alluvial valleys, the valley shape irregular shape and shear wave velocity as the type of material specification must be considered. Therefore, in this study, the results and magnification charts are presented to clarify the seismic response of irregular alluvial valleys of triangular shape. The analysis in the time domain was performed using the method of the SFEM and NASEM software. The results of this study show that the natural frequency of the irregular triangular valley decreases and reaches the natural frequency of the soil layer applied to the rocky bed (one-dimensional) with decreasing slope of the valley.

Each irregular triangular valley has a natural frequency and the magnification value of each single point in the valley changes with variations in the slope of the valley. So, the magnification pattern of irregular valleys are highly dependent on the variations or irregularity degree of alluvial valley, the maximum magnification values increase and by decreasing the slope of the irregular valley, which is maximum for the angle of 15 degrees in the valley slope. On the other hand, the magnification value decreases with increasing shear wave velocity in the medium. The largest magnification values occur in the area of the valley, which weighs more than alluvial. The valley's natural frequency increases with increasing the velocity of the shear wave in the environment. The natural frequency of a triangular valley is obtained from the following equation when a side of the valley has a gradient angle of 45°:

$$f = (-2E - 7 \times \beta^4 + 3E - 5 \times \beta^3 - 0.0017 \times \beta^2 + 0.0703 \times \beta + 1) \times V_s / (4H) \quad (14)$$

In which β is slope angle, V_s is the shear wave velocity, and H is the maximum layer thickness of irregular triangular alluvial valley.

5. Conflicts of Interest

The authors declare no conflict of interest.

6. References

- [1] Ohtsuki, Akira, and Kasaburo Harumi. "Effect of topography and subsurface inhomogeneities on seismic SV waves." *Earthquake Engineering & Structural Dynamics* 11, no. 4 (1983): 441-462. doi: 10.1002/eqe.4290110402.
- [2] Ohtsuki, Akira, Hiroshi Yamahara, and Takashi Tazoh. "Effect of lateral inhomogeneity on seismic waves, II. Observations and analyses." *Earthquake engineering & structural dynamics* 12, no. 6 (1984): 795-816. doi: 10.1002/eqe.4290120607.
- [3] Chuhan, Z., & Chongbin, Z. (1988). Effects of canyon topography and geological conditions on strong ground motion. *Earthquake engineering & structural dynamics*, 16(1), 81-97. doi: 10.1002/eqe.4290160107.
- [4] Sohrabi - Bidar, A., M. Kamalian, and M. K. Jafari. "Time - domain BEM for three - dimensional site response analysis of topographic structures." *International journal for numerical methods in engineering* 79, no. 12 (2009): 1467-1492. doi: 10.1002/nme.2619.
- [5] Ling Ning , Tianyu Dai , LiminWang , Shichuan Yuan , Jingyin Pang, "Numerical investigation of Rayleigh-wave propagation on canyon topography using finite-difference method", *Journal of Applied Geophysics* 159 (2018) 350–361. doi: 10.1016/j.jappgeo.2018.09.007.
- [6] Zezhong Zhang, Jean-Alain Fleurisson, Frederic Pellet, "The effects of slope topography on acceleration amplification and interaction between slope topography and seismic input motion", *Soil Dynamics and Earthquake Engineering* 113 (2018) 420–431. doi: 10.1016/j.soildyn.2018.06.019.
- [7] Reinoso E, Wrobel LC, Power H, 1997. Twodimensional scattering of P, SV and Rayleigh waves: preliminary results for the valley of Mexico. *Earthquake Engineering and Structural Dynamics*, 26: 595–616. doi: 10.1002/(sici)1096-9845(199706)26:6%3C595::aid-eqe657%3E3.0.co;2-s.
- [8] Tadeo A, Santos P, Antonio J, 2001. Amplification of elastic waves due to point source in the presence of complex surface topography. *Computers and Structures*, 79: 1697–1712. doi: 10.1016/s0045-7949(01)00098-0.
- [9] Kavand, Ali, Sarkashkzadeh Motlagh, Sayed Ahmad, & Qalandarzadeh, "Seismic response of alluvial deposits due to vertical component of earthquake near fault zone". *Quarterly Journal of Earthquake Engineering Sciences* 3, no. 2, 2016: 1-20.
- [10] Najafizadeh, Jafar. (2014). Investigation of seismic nonlinear behavior of two dimensional alluvial valleys with the help of finite element spectra (PhD thesis). International Institute of Seismology and Earthquake Engineering. Tehran.
- [11] Najafizadeh, Jafar, Mohsen Kamalian, Mohammad Kazem Jafari, and Naser Khaji. "Seismic analysis of rectangular alluvial valleys subjected to incident SV waves by using the spectral finite element method." *Int J Civ Eng* 12, no. 3 (2014): 251-263.